

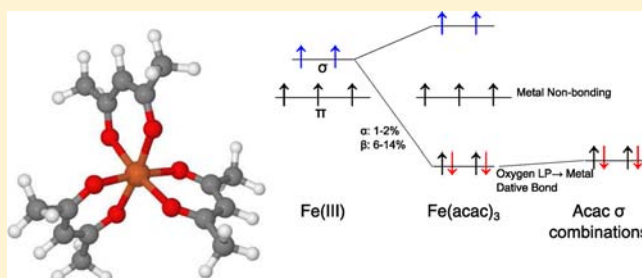
Theoretical Investigation of Paramagnetic NMR Shifts in Transition Metal Acetylacetonato Complexes: Analysis of Signs, Magnitudes, and the Role of the Covalency of Ligand–Metal Bonding

Ben Pritchard and Jochen Autschbach*

Department of Chemistry, State University of New York at Buffalo, Buffalo, New York 14260-3000, United States

Supporting Information

ABSTRACT: Ligand chemical shifts are calculated and analyzed for three paramagnetic transition metal trisacetylacetonato (acac) complexes, namely high-spin Fe(III) and Cr(III), and low-spin Ru(III), using scalar relativistic density functional theory (DFT). The signs and magnitudes of the paramagnetic NMR ligand chemical shifts are directly related to the extent of covalent acac oxygen-to-metal σ donation involving unoccupied metal valence d_{σ} acceptor orbitals. The role of delocalization of metal-centered spin density over the ligand atoms plays a minor secondary role. Of particular interest is the origin of the sign and magnitude of the methyl carbon chemical shift in the acac ligands, and the role played by the DFT delocalization error when calculating such shifts. It is found that the α versus β spin balance of oxygen σ donation to metal valence d acceptor orbitals is responsible for the sign and the magnitude of the ligand methyl carbon chemical shift. A problematic case is the methyl carbon shift of Fe(acac)₃. Most functionals produce shifts in excess of 1400 ppm, whereas the experimental shift is approximately 279 ppm. Range-separated hybrid functionals that are optimally tuned for Fe(acac)₃ based on DFT energetic criteria predict a lower limit of about 2000 ppm for the methyl carbon shift of the high-spin electronic configuration. Since the experimental value is based on a very strongly broadened signal it is possibly unreliable.



1. INTRODUCTION

In recent years the accurate prediction, from first principles theory, of NMR spectra of compounds with unpaired electrons (paramagnetic NMR, or short: pNMR) has gained increasing attention. The systems of interest are often metal complexes that are large by quantum chemistry standards in terms of the number of required basis functions and/or number of electrons, and (for heavier elements) due to the need of a relativistic quantum theoretical framework. In a commonly adopted approximation,^{1–5} pNMR chemical shifts involve separate calculations of regular NMR shielding, which is caused by magnetic-field induced orbital current densities, as well as g and hyperfine (A) “tensors” (as they are commonly termed) encountered in electron paramagnetic resonance (EPR) spectroscopy. The resulting pNMR shifts can be written as a sum of pseudocontact shifts related to the anisotropy of the magnetic susceptibility tensor (including through-space magnetic interactions of the paramagnetic center with the ligand nuclei), contact shifts that result from nonvanishing spin density at the nucleus of interest, and the “regular” orbital current-density induced shielding. Zero-field splitting may also influence paramagnetic NMR shifts. Theoretical predictions of NMR and EPR parameters demand inclusion of electron correlation to some degree, and more generally a high-quality computational model that may have to include solvent effects. It is therefore no surprise that the bulk of recently published

work has relied on density functional theory (DFT) because of its efficient treatment of electron correlation and the availability of relativistic methods for NMR and EPR parameters.^{2,3,6,7}

However, commonly used density functionals afford approximations that may hamper accurate predictions of pNMR chemical shifts. In particular for open-shell metal complexes with large ligand contact shifts, the delocalization error of DFT⁸ must be considered as a significant problem. The reason is that too covalent metal–ligand bonding furnished by nonhybrid and many hybrid functionals may lead to an overly delocalized spin density “leaking” from the paramagnetic metal center to the ligand atoms or vice versa. A too localized electronic structure, on the other hand, may underestimate the covalent character of metal–ligand interactions and likewise lead to poor agreement of calculated pNMR shifts with experiment. It has long been recognized that DFT tends to overestimate the covalent character of ligand–metal bonding.^{9,10} The dependence of calculated shifts on the functional has been previously noted. For instance, Liimatainen et al. have stated that “...the selection of the exchange-correlation functional was found to be a crucial factor in determining the accuracy of the predicted shifts.”¹¹

Received: April 27, 2012

Published: July 26, 2012

pNMR spectra are not as intuitively interpreted as typical diamagnetic NMR spectra. One reason is the lesser amount of available experimental and theoretical information compared to the huge body of data for diamagnetic NMR. Another reason is that paramagnetic effects from the unpaired electron spin density can range from very large to (almost) negligible, and that they can vary in sign among atoms in the same molecule or complex or between structurally closely related systems. For the purpose of establishing reliable computational protocols, and for the purpose of gaining a better chemical understanding of how structure and bonding determine pNMR shifts, it is advantageous to investigate a series of structurally related compounds. For instance, calculations of ligand pNMR shifts for 3d metallocenes MCp_2 with $M = \text{V}, \text{Cr}, \text{Mn}, \text{Co}, \text{Ni}$, and $\text{Cp} = \text{cyclopentadienyl}$ using DFT with pure and hybrid functionals have been reported.^{12,13} pNMR shifts calculated with hybrid functionals were shown to reproduce experimental ^{13}C and proton chemical shifts very well over the accessible shift ranges (which cover 2000 ppm for carbon and about 570 ppm for protons). With the help of newly developed hyperfine coupling analyses in terms of localized molecular orbitals (LMOs), we have recently shown how shielding trends within the metallocene series can be understood in terms of a balance between α and β spin orbitals involved in covalent ligand–metal σ and π interactions.¹³ The spatial extensions of the metal 3d orbitals among the set of metals was also shown to play an important role. As an example, the LMO analysis demonstrated that the large positive ^{13}C shifts for nickelocene (expt. around 1514 ppm) are caused predominantly by charge donation from Cp β -spin orbitals to unoccupied metal β -spin 3d orbitals ($3d^\beta$), leaving an excess of α -spin density in the ligand π system. For vanadocene, negative ^{13}C shifts of about -510 ppm were shown to be caused predominantly by the interaction of the occupied $3d^\alpha$ orbital with Cp orbitals, causing a strong spin polarization of the carbon 1s shells toward excess β density which ends up dominating the result.

Another set of paramagnetic systems that has garnered significant experimental and computational interest is comprised of transition metal acetylacetonato (acac) complexes shown in Figure 1. For instance, Eaton discussed the role of

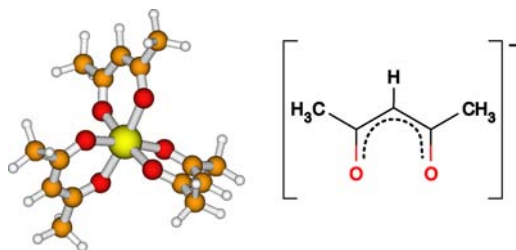


Figure 1. Representative structure of a metal acetylacetonato (acac) complex.

charge transfer and bonding in the proton NMR spectra of several such complexes,¹⁴ and experimental shifts and NMR linewidths have been measured by Doddrell and Gregson.¹⁵ Computations were performed recently by Rastrelli and Bagno (RB).^{2,3} See also ref 16. There are interesting trends in the data set that warrant analysis by means of first-principles theoretical calculations. An example is the opposing sign of the methyl carbon shift for $\text{Fe}(\text{acac})_3$ (positive) versus $\text{Cr}(\text{acac})_3$ (negative) or $\text{Ru}(\text{acac})_3$ (negative), along with strongly differing magnitudes of these shifts (experimentally 21 to 279

ppm). Further, the Ru complex affords negative calculated methyl proton pNMR shifts whereas those in $\text{Fe}(\text{acac})_3$ and $\text{Cr}(\text{acac})_3$ are positive. What details of the covalent metal–ligand interactions could be responsible for the sign changes?

Another important aspect is the agreement of calculations with experiment. RB obtained reasonable calculated ^1H pNMR shifts for $\text{Cr}(\text{III})$, high-spin $\text{Mn}(\text{III})$, high-spin $^{14}\text{Fe}(\text{III})$, $\text{Cu}(\text{II})$, and low-spin $\text{Ru}(\text{III})$ acac complexes using DFT.^{2,3} The reported ^{13}C shifts obtained from DFT calculations, however, deviated substantially from experiment. In particular, the chemical shift of the methyl carbons in $\text{Fe}(\text{acac})_3$ was predicted to be over 2400 ppm, which is an order of magnitude larger than the experimental shift of 279.3 ppm.¹⁵ This disparity was hypothesized by RB to be due to an overly broad experimental signal, rendering the experimental shift value unreliable. This assessment was supported with theoretical estimations of the line widths. It is quite possible, however, that the discrepancy, or part of it, is caused by deficiencies in the calculations since NMR and EPR parameters of 3d metal complexes are notoriously difficult to predict with DFT.^{17,18} Therefore, the case of $\text{Fe}(\text{acac})_3$ warrants a detailed investigation in order to elucidate the precise factors controlling the accuracy of the methyl carbon shift, and possible inadequacy in the electronic structure with respect to those factors.

We report herein LMO analyses of pNMR shifts, and a systematic investigation of the influence of the DFT delocalization error, for tris-acetylacetonato $\text{Fe}(\text{III})$, $\text{Cr}(\text{III})$, and $\text{Ru}(\text{III})$. The LMO analyses produce chemically intuitive contributions to the (dominant) contact shifts in these complexes in terms of bonding, lone-pair or nonbonding, and core orbitals. One aim of this work is the explanation of the sign relations among the methyl carbon chemical shifts between different complexes by utilizing the LMO analysis. Another aim is to quantify how the various contributions to the ligand pNMR shifts, particularly from metal 3d orbitals, are altered when different functionals with different degrees of the delocalization error are employed. To this end, we investigate the performance of “pure” (nonhybrid), standard global hybrid, and exchange range-separated hybrid functionals (“coulomb attenuated” (CAM) or long-range corrected (LC) functionals). The delocalization error is quantified via the curvature of $E(N)$, the energy as a function of the fractional electron number.⁸

Computational details are provided in section 2. The results of the NMR computations and the LMO analyses are reported and discussed in section 3. A brief summary and an outlook in section 4 concludes this Article.

2. COMPUTATIONAL DETAILS

Geometries were optimized with the Amsterdam Density Functional (ADF)¹⁹ program using the BP^{20,21} functional, the scalar all-electron zeroth-order regular approximation (ZORA),²² and a doubly polarized triple- ζ (TZ2P) Slater-type basis set from the ADF basis set library, and employed spin-unrestricted DFT. Hyperfine tensors, g tensors, and shielding tensors were calculated using a locally modified 2011 developer’s version of the open source NWChem package^{23,24} including recently developed ZORA functionality for hyperfine coupling, and ZORA-based gauge-including atomic orbital (GIAO) methods for NMR shielding and g -shifts.^{25–27} A fully uncontracted ANO-RCC Gaussian-type basis set²⁸ (ANO) was used on the metal center, and IGLO-III²⁹ for the ligand atoms. Additional technical details of the NWChem ZORA pNMR calculations can be found in refs 13 and 27. For benchmarking purposes and further validation of the methods, pNMR calculations were also carried out with a locally

Table 1. pNMR Shift for Fe(acac)₃ Calculated with $S = 5/2$ and $T = 305$ K. $\Delta g_{\text{iso}} = g_{\text{iso}} - g_e$ in Parts per Thousand (ppt). NWChem (NW) and ADF Calculations

	NW BP	NW PBE	NW B3LYP	NW PBE0	NW BHLYP	NW CAM	NW LC-PBE0	NW HF
Δg_{iso}	10.00	9.77	7.01	5.70	2.77	5.45	3.77	0.12
methyl H	46.67	44.43	18.82	13.02	4.08	14.13	9.75	-10.81
methyl C	2773	2759	2156	1947	1457	1907	1597	776.8
methine H	50.41	50.84	1.20	-3.31	-19.33	-10.28	-11.85	-22.70
methine C	2256	2280	1614	1391	916	1307	1001	369.5
carbonyl C	1130	1096	766.3	700.3	596.6	848.6	848.8	301.2
	ADF BP	ADF PBE	ADF PBE0	ADF BHLYP	ADF HF	RB ^a	expt	
Δg_{iso}	10.45	10.37	5.88	2.85	0.11	253.0	$\approx 0^b$	
methyl H	48.58	51.08	15.79	4.07	-13.69	24.13	21.5, ^c 21.8 ^{d,e}	
methyl C	2815	2852	1983	1489	818.8	2447	279.3 ^d	
methine H	36.37	48.89	-4.68	-22.57	-26.68	-2.04	-29.7, ^c -27.4 ^d	
methine C	2358	2397	1432	941.7	396.7	1715		
carbonyl C	1061	1145	754.0	621.5	274.8	959.2		

^aGaussian 03/B3LYP, cc-pVTZ (C,H,O), and 6-31G(d,p) (Fe). Reference 2. ^bReference 49. ^cReference 2. ^dIn CDCl₃, $T = 305$ K. Reference 15. ^eIn CDCl₃, $T = 305$ K. Reference 50.

modified developer's version of the Amsterdam Density Functional (ADF) package using the ZORA pNMR methods reported in refs 16 and 30. The ADF NMR and EPR calculations employed the "JCPL" Slater-type basis set for ligand atoms³¹ and the QZ4P basis set from the ADF basis set library for the metal centers. The calculations generally converged to solutions with reasonable $\langle S^2 \rangle$ expectation values, indicating that the amount of spin-contamination is small. The $\langle S^2 \rangle$ values ranged for Fe from 8.7546 to 8.7579 (expected 8.7500), for Cr from 3.7606 to 3.7730 (expected 3.7500), and for Ru from 0.7552 to 0.7578 (expected 0.7500, with HF theory producing an outlier with a value of 0.7712). We note that it is important to perform the calculations of the ligand hyperfine tensors with spin-unrestricted DFT because of the important mechanism of spin-polarization to produce negative contact spin densities at ligand atoms even if the overall $\langle S_z \rangle$ is positive.³²⁻³⁴

Following refs 1 and 27, pNMR chemical shifts were calculated using eq 1

$$\sigma = \sigma^{\text{orb}} - \frac{\beta_e}{g_N \beta_N} \frac{S(S+1)}{3kT} \mathbf{g} \mathbf{A}^T \quad (1)$$

where the g -tensor \mathbf{g} , hyperfine tensor \mathbf{A} , and orbital shielding tensor σ^{orb} were obtained with the NWChem and ADF codes, respectively, for spin S . The constants β_e , β_N , and g_N represent the Bohr magneton, nuclear magneton, and nuclear g -value, respectively. In this formalism, contact shifts are associated with the isotropic hyperfine coupling constant (HFCC, the isotropic average of \mathbf{A}). The NMR and EPR tensors were calculated using second-order perturbation theory.^{16,30} These parameters were combined to arrive at the total isotropic pNMR nuclear shielding constant by using eq 1 and taking the isotropic average. When used in eq 1, the hyperfine tensor has been modified to incorporate the g -tensor rather than the g_e value.¹⁶ However, this correction is not applied to the tensors as used in the LMO analyses. Due to the small g -shifts the difference is not significant. See the Supporting Information (SI) for corrected and uncorrected isotropic HFCC values. For additional details on calculation of pNMR shifts, see our previous publications^{13,16,30} and refs 17, 35, and 36. The pNMR shielding constants were converted to chemical shifts via $\delta = \sigma^{\text{ref}} - \sigma$ using the ¹H and ¹³C shielding constants (σ^{ref}) of the reference molecule tetramethylsilane (TMS) calculated in an identical fashion to those of the complexes (for TMS only the σ^{orb} term is relevant). The calculations showed that the paramagnetic effects were dominated by the isotropic ligand HFCCs. The LMO analysis of the HFCCs proceeded on the basis of orbital localizations carried out with the NBO 5.0 program,^{37,38} using the analysis protocol and software detailed in ref 13. The NBO algorithms by design create sets of LMOs corresponding to one of different possible Lewis structures. For a strongly delocalized system, changes in

the functional or slight distortions in the local symmetry of different ligands may favor one Lewis structure over another. Switching from one Lewis structure to another results in a concomitant redistribution of contributions from different LMOs to the calculated HFCCs (or other properties analyzed with these LMOs). The analysis can be averaged over equivalent Lewis structures as has been done previously in studies of diamagnetic NMR chemical shifts and J -coupling as well as electric-field gradients,³⁹⁻⁴¹ but the protocol is somewhat time-consuming and has therefore not been adopted for the present study.

For systems with more than one unpaired electron ($S > 1/2$), zero-field splitting (ZFS) is potentially important.^{11,42} The factor $S(S+1)/3$ (times a unit matrix, between \mathbf{g} and \mathbf{A}^T) in eq 1 is obtained from Boltzmann averaging $\langle m_i \hat{S}_i \hat{S}_i m_i, S \rangle$ for the ground-state multiplet in the absence of magnetic fields, assuming that the states have degenerate energies. \hat{S}_i is here the effective spin operator of the EPR spin-Hamiltonian. In the presence of ZFS, the Boltzmann averaging needs to be done with the eigenfunctions and eigenvalues of the ZFS Hamiltonian. For high-spin metallocene complexes, a simplified treatment of ZFS in paramagnetic NMR has been shown to give negligible contributions to ligand pNMR shifts.¹² A more complete treatment of ZFS in pNMR calculations has shown that the magnitude is often small compared to variations of calculated pNMR shifts with respect to functionals, but should be included for a complete description.¹¹ To test if ZFS is of importance for the acac complexes studied here, the ZFS tensors for Fe(acac)₃ and Cr(acac)₃ were calculated with ADF^{43,44} (PBE functional). The calculated ZFS tensor elements were found to be very small (see the SI). A calculation of the pNMR shifts including the ZFS tensor using the formalism of Penannen and Vaara⁴² found no significant differences with the results obtained from eq 1. Therefore, in the present study the ZFS has been neglected.

Functionals used in this work include BP (Becke88²⁰ exchange and Perdew86²¹ correlation), the B3LYP functional⁴⁵ with 20% exact exchange, the 50% global hybrid BHLYP,⁴⁶ a hybrid version (PBE0) of the Perdew–Burke–Ernzerhof (PBE) functional²¹ with 25% exact exchange, PBE itself, and the default parametrization of the range-separated hybrid functional CAM-B3LYP (or short: CAM)⁴⁷ which affords 19% exact exchange at short interelectronic distances and 65% asymptotically. As a representative of the class of fully long-range corrected functionals, we employed the LC-PBE0 parametrization of a range-separated PBE hybrid variant as used previously in ref 48.

3. RESULTS AND DISCUSSION

This section first reports results from Fe(acac)₃ pNMR shift calculations, followed by a discussion of the DFT delocalization error for this complex and the LMO analysis of the methyl carbon hyperfine coupling. Subsequently, Cr(acac)₃ and

$\text{Ru}(\text{acac})_3$ are analyzed and discussed in relation to the iron complex. We then return to $\text{Fe}(\text{acac})_3$ and investigate how the functional might be systematically improved.

3.1. Chemical Shifts of $\text{Fe}(\text{acac})_3$. pNMR ligand shifts for high-spin $\text{Fe}(\text{acac})_3$ calculated with a variety of functionals are collected in Table 1. Calculated shifts were found to be equivalent for symmetry-equivalent atoms. This is to be expected for a molecule with a spatially nondegenerate electronic state. Although the basis sets and many technical aspects between NWChem and ADF differ, the results between the two software packages are comparable for the same functional and the same relativistic Hamiltonian, which is reassuring. Note that scalar relativistic effects for light ligand atoms in 3d metal complexes tend to be small but were included here for consistency with our recent work on EPR parameters and pNMR shifts.^{13,16,30} The good agreement between the two codes indicates that the chosen basis sets are adequate for the pNMR calculations.

Overall, the order of magnitudes of pNMR shifts for different atom types in the complex agrees with those reported by RB (B3LYP functional), but the numerical values differ. There are several possible reasons for the observed discrepancies. The Δg_{iso} calculated with ZORA differs noticeably from the RB value; we note that our isotropic g is close to experiment ($\Delta g_{\text{iso}} \approx 0$, $g_{\text{iso}} \approx g_e$).⁴⁹ Starting from variationally stable scalar ZORA ground states, the calculations employ the variationally stable ZORA variant of the spin-orbit (SO) coupling operator for the SO perturbation in the g -tensor. The electron Coulomb potential in the SO operator affords an approximate mean-field treatment of certain two-electron terms that partially compensate the nuclear potentials. The calculations performed by RB might have overestimated the SO coupling in the complex, as indicated by the too large g -shift. Further, the basis set used on the ligands in this work (IGLO-III) was originally designed for calculation of NMR parameters and, for carbon, contains basis functions with exponents ranging to roughly twice that of the highest exponent in the cc-pVTZ basis used by RB. Therefore, IGLO-III is likely better suited for properties based on operators that are large close to a nucleus, such as nuclear shielding and HFCC.^{13,16} We note that our optimized geometry was found to be nearly identical to the geometry published by RB.²

From the calculations on the $\text{Fe}(\text{acac})_3$ complex, it is clear that pure functionals (BP and PBE) perform poorly. The methyl proton shifts are overestimated by up to 30 ppm, and the shifts for the CH protons are of the wrong sign. Global hybrid functionals and hybrid functionals with range-separated exchange improve the calculations to a reasonable degree, correcting the sign on the CH proton shifts and bringing all proton shifts closer to experiment. By far the largest disagreement lies with the methyl ^{13}C shift (the only carbon, unfortunately, for which experimental NMR data are available). This discrepancy has previously been associated with the large line-width observed in the experimental data (approximately 1800 Hz).^{2,15} However, the large variations of the calculated shifts for this nucleus among the set of functionals also point to deficiencies in the electronic structure model as a possible reason for the discrepancy. The calculated pNMR shifts of all nuclei in $\text{Fe}(\text{acac})_3$ are almost exclusively caused by the contact mechanism which originates from nonvanishing spin density at the ligand nuclei. The orbital shieldings remain relatively constant on the scale of the pNMR shifts in the complex, and the g -tensor is nearly equivalent across all functionals and

remains close to the isotropic free-electron case. As a result of the small g -shifts, contributions to the pNMR chemical shifts other than the contact terms were found to be negligible, in agreement with previous estimates.^{2,15}

All density functionals appear to perform inadequately for the methyl carbon shifts, overestimating the experimental shift by an order of magnitude. On the basis of the above discussion, this is entirely due to an excessively large isotropic HFCC calculated for the methyl carbons. The agreement with the experimental estimate of 279 ppm is worst for pure functionals, overestimating by about 2500 ppm. The difference is noticeably reduced with hybrid functionals, with B3LYP predicting a methyl ^{13}C shift of about 1500 ppm. Hartree-Fock (HF) calculations reduce this difference further by a significant amount. The trend is very clear that agreement with the experimental shift for the methyl carbon is improved for large fractions of exact exchange in the functional, although such high percentages of HF can harm agreement with respect to proton shifts. The range-separated hybrid functionals CAM-B3LYP and LC-PBE0 show some improvements over their global-hybrid counterparts, but not spectacularly so.

One may wonder if, at the temperature of the NMR experiment, there is a mixture of high-spin and low-spin electronic states present. However, some experimental ESR data recorded over a range of 82–302 K indicated that the complex is in the high-spin state.⁴⁹ The experimental NMR spectrum was taken at approximately 305 K, at the upper end of this temperature range.¹⁵ A geometry optimization was carried out on the low-spin configuration in a fashion equivalent to that stated in the Computational Details section. A comparison of the energy calculated with ADF and a B3LYP functional employing 15% HF exchange (which has been recommended previously for spin-crossover studies⁵¹) found an energy difference of 0.2 eV or about 20 kJ/mol, with the high-spin complex having lower energy. While relative energies of spin states are notoriously difficult to predict with DFT, the energy separation does not point to a significant population of the low-spin state at 305 K. It therefore seems unlikely that the low-spin complex contributes significantly to the NMR spectrum at 305 K. However, there are experimentally observed anomalies for this complex. Vlieg and Zandstra noted significant temperature-dependent Faraday C terms in the magnetic circular dichroism spectrum.⁵² Gregson et al. also noted some anomalies in the temperature dependence of the ^1H spectrum of $\text{Fe}(\text{acac})_3$. Because of the small ZFS, the origin of the temperature dependence was not clear.⁵³ We note in passing that the methyl carbon shift calculated for the low-spin configuration is negative (−129 ppm, obtained with the BP functional and the ADF implementation); i.e., it has the same sign as the corresponding shift in the low-spin Ru(III) complex but is larger in magnitude.

3.2. Delocalization Errors and $E(N)$ for $\text{Fe}(\text{acac})_3$. DFT with approximate functionals typically affords delocalization errors⁸ (more traditionally discussed in the context of “self-interaction”) which may affect the extent to which spin-density originating at the metal reaches into the ligands or vice versa. The delocalization error can be quantified by calculating the energy $E(N)$ of a system as a function of fractional electron number N . We recently implemented fractional electron-number DFT calculations in NWChem^{48,54} which allows us here to study delocalization errors in the functional used for calculating the pNMR shifts of the acac complexes. The correct behavior of $E(N)$ is to vary linearly both in electron deficient ($\Delta N = N - N(\text{neutral}) < 0$) and electron rich ($\Delta N > 0$)

regimes, with the slope of $E(N)$ changing abruptly at $\Delta N = 0, \pm 1, \pm 2, \dots$ (derivative discontinuity⁵⁵). Therefore, any nonvanishing curvature of $E(N)$ may be correlated with the delocalization error of a particular functional for a given molecule or complex.

For the acac complexes studied in this work, it is important to keep in mind that there is intraligand delocalization (especially physically meaningful delocalization in the ligand π system) and delocalization associated with the covalent nature of the ligand–metal interactions. Because of the unrestricted nature of the calculations, occupations can be varied in either the α or β sets of orbitals. Results for calculations of $E(N)$ of $\text{Fe}(\text{acac})_3$ in the β set is provided in Figure 2. This graph demonstrates that all functionals afford

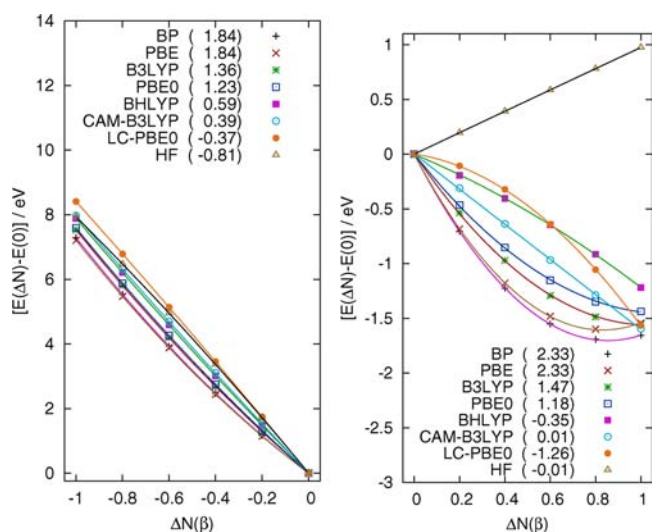


Figure 2. Energy $E(\Delta N)$ of $\text{Fe}(\text{acac})_3$ as a function of fractional β -spin electron number $\Delta N(\beta)$. The value of $\Delta N(\beta) = 0$ corresponds to the neutral system while $\Delta N = \pm 1$ represents the anion/cation. Numbers in parentheses are the coefficients of the ΔN^2 terms of quadratic fits for $E(N)$.

noticeable curvatures and therefore significant delocalization errors in the $\text{Fe}(\text{acac})_3$ electronic structure. As a general trend, it emerges that functionals (including HF) exhibiting the least amount of curvature in the $E(N)$ plots tend to perform better in calculations of the pNMR chemical shifts. The correspondence is not perfect; for instance, on the basis of the curvature parameters, CAM-B3LYP should perform better than BHLYP,

but if the experimental shift for the methyl carbon is reliable then BHLYP performs somewhat better. However, CAM-B3LYP does perform better than pure functionals which exhibit particularly large curvatures in the $E(N)$ plots.

There is some question as to whether $E(N)$ for varying ΔN in the α set or the β set is more important. The β set of spin orbitals may be more appropriate for assessing the functional performance, since the calculated electron affinities $E(\Delta N = 1) - E(\Delta N = 0)$ are reasonably close to the experimental value of 1.87 ± 0.10 eV.⁵⁶ The β -spin LUMOs, in particular, have large metal d character (see the SI). Therefore, the electron-rich $\Delta N(\beta)$ plots may be particularly indicative of delocalization errors affecting the dative covalent ligand–metal interactions. However, for distant nuclei such as the methyl carbons there is also a question of whether too little delocalization in the ligands describes the ligand-centered orbitals poorly. When varying the β -spin electron number, HF gives nearly a perfectly straight line in the $\Delta N > 0$ segment. However, the slope is opposite to all density functionals, and HF gives an unrealistic electron affinity of -1.0 eV. The corresponding orbital is of diffuse nature unlike those obtained from the DFT calculations. Therefore, it is questionable whether the lack of curvature of $E(N)$ for this plot segment is related to the performance of HF in the pNMR calculations. All density functionals show a significant degree of curvature in $E(N)$ for the β -spin $\Delta N > 0$ segment, pointing to a possible underlying problem with electron delocalization. The only density functionals for which negative curvature indicates too little delocalization are LC-PBE0 (which, as pointed out above, may adversely affect the spin-density distribution in the ligands) and, to a much lesser degree and only for $\Delta N(\beta) > 0$, BHLYP.

3.3. Orbital Analysis. In this subsection, a more detailed analysis is provided for the $\text{Fe}(\text{acac})_3$ methyl carbon pNMR shift. Because the variations among the functionals are strongly dominated by the pNMR contact terms, the analysis of the factors controlling the ^{13}C shielding focuses on that term, which considerably simplifies the discussion. The contact shift is directly proportional to the isotropic HFCC. As it will be shown, the extent of ligand oxygen-to-metal dative bonding plays a major role. Due to the unrestricted nature of the calculations, it is necessary to discuss these covalent interactions not as dative electron-pair bonds but rather as α and β spin pairs of partially covalent one-electron bonds.

Contributions to the HFCC from equivalent localized occupied α and β orbitals with identical spatial components are equivalent but have opposite signs. A nonvanishing ligand

Table 2. LMO Contributions to the Calculated Methyl Carbon HFCC for $\text{Fe}(\text{acac})_3$ in MHz Calculated with NWChem ANO/IGLO-III/ZORA

LMO type	BP	PBE	B3LYP	PBE0	BHLYP	CAM	LC-PBE0	HF
C core	0.791	0.790	0.709	0.663	0.553	0.628	0.562	0.322
C–C NN σ bond	0.811	0.798	0.637	0.564	0.422	0.551	0.442	0.201
methyl C–H σ bond	−0.352	−0.334	−0.254	−0.229	−0.144	−0.196	−0.157	−0.063
Fe–O σ bond ^b (nearest ^a)	0.954	0.965	0.800	0.762	0.724	0.755	0.746	0.573
nearest ^a O LP	−0.230	−0.250	−0.315	−0.329	−0.445	−0.321	−0.374	−0.483
metal SOMOs	0.113	0.112	0.067	0.059	0.041	0.053	0.045	0.024
other	0.179	0.174	0.115	0.102	0.035	0.086	0.037	0.048
sum of analysis	2.266	2.255	1.759	1.592	1.186	1.556	1.301	0.622
total calcd	2.264	2.253	1.759	1.590	1.187	1.556	1.301	0.624

^a“Nearest” refers to the spatially closest of the two carbonyl groups in the same ligand. NN = nearest neighbor. ^bFe–O bond formally exists only in the β set.

atom hyperfine coupling is then determined (i) by contributions from formally unpaired orbitals that are not compensated by an opposite-spin partner orbital, and (ii) by HFCC contributions from pairs of equivalent α and β LMOs that do not completely cancel because of spin-polarization of the system. The analysis results are collected in Table 2, and the trends are graphically displayed in Figure 3. For brevity, in the

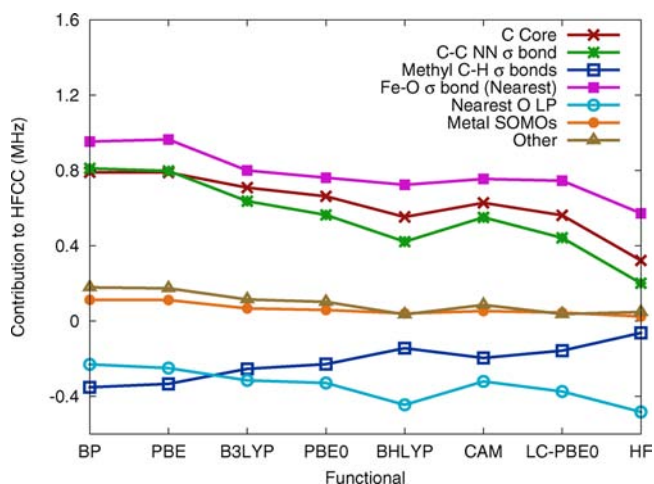


Figure 3. LMO contributions to the calculated methyl carbon HFCC for $\text{Fe}(\text{acac})_3$. See Table 2 for details. Lines connecting the data points were added for better readability.

following discussion “bond” is occasionally used as shorthand for “bonding LMO”. Likewise, “lone pair” refers to a lone-pair (one-center or metal nonbonding) LMO, and “core” to core LMOs.

In the high-spin $\text{Fe}(\text{acac})_3$ complex, the five occupied unpaired $\text{Fe } d^\alpha$ orbitals are formally nonbonding. A small degree of covalent interaction of the d_x^2 (corresponding to the set of t_{2g} metal orbitals in octahedral parent symmetry) with unoccupied ligand π^* orbitals is the likely cause for the small positive metal SOMO contributions to the methyl carbon HFCC. The ligand π system, as well as the C–O π bond, both do not contribute *directly* to the hyperfine coupling. Therefore, these LMOs are not explicitly listed in Table 2. The analysis points to partially covalent dative O \rightarrow Fe σ bonds as a strong source for the methyl HFCC. Since the metal d^α spin-orbitals are all occupied, the dative bond can only formally occur

between oxygen β lone-pairs of local σ symmetry and empty $\text{Fe } d_\sigma^\beta$ orbitals. From the LMO analysis, the depletion of β density at the oxygen centers is seen to propagate through the ligand system, causing the overall positive HFCC at the methyl carbon.

No LMO contribution can be singled out as being the only cause of the large methyl carbon HFCC. Most LMOs yield a positive contribution to the HFCC. Since the functionals are all different, no monotonous trend should be expected *a priori*. However, there is a clear overall trend in Figure 3 that the contributions from all LMOs decrease with increasing global fraction of HF exchange as well as upon the inclusion of long-range HF exchange in the range-separated hybrids CAM-B3LYP and LC-PBE0. The lone exception to the trend is the negative contribution from the methyl C–H σ bonds, which increases in a roughly mirror-image manner compared to the other contributions. The contributions from the C–C nearest-neighbor σ bonds and the O \rightarrow Fe bonding LMOs show the largest absolute decrease upon varying the functional. It is noted that BHLYP and LC-PBE0 behave very similarly. It appears that long-range exact exchange is beneficial, and that global hybrid functionals that include large amounts of HF (50% for BHLYP) can mimic such corrections to some degree. Overall, the reduction of the magnitude of practically all relevant LMO contributions to the methyl HFCC upon increasing fraction of exact exchange in the functional follows qualitatively the trend for the delocalization errors quantified by the curvature of $E(N)$ (section 3.2). An exception is the large negative curvature for $E(N)$ for LC-PBE0 upon increasing the β -spin occupation where the correct long-range behavior of the potential possibly renders the functional too “Hartree–Fock-like”.

Plots of selected LMOs for $\text{Fe}(\text{acac})_3$ can be found in the SI. The plots indicate that electron density from ligand-centered orbitals other than the β O \rightarrow Fe bonds delocalizes onto the metal center, but mainly so only in the β -spin set. Delocalization of the carbon–oxygen π bond would represent ligand–Fe π donation. A mixing of occupied ligand with unoccupied metal orbitals is also apparent in other orbitals, such as the formally nonbonding oxygen lone-pair. The delocalization is particularly noticeable for the nonhybrid BP functional and decreases with increasing HF exchange. The corresponding α spin LMOs remains well-localized for all functionals.

Table 3. Metal Contributions to Selected LMOs in $\text{Fe}(\text{acac})_3$ ^a

	BP	LC-PBE0	BHLYP	HF
π (C–O) α	0.05%	0.05%	0.04%	0.06%
	s(1) p(14) d(27) f(58)	s(1) p(15) d(32) f(52)	s(1) p(13) d(35) f(51)	s(1) p(8) d(62) f(30)
β	2.81%	2.27%	2.08%	1.36%
	s(0) p(0) d(99) f(1)	s(0) p(0) d(99) f(1)	s(0) p(0) d(99) f(1)	s(0) p(0) d(98) f(1)
O LP α	0.69%	0.51%	0.51%	0.40%
	s(92) p(2) d(5) f(2)	s(87) p(1) d(9) f(2)	s(86) p(1) d(10) f(2)	s(76) p(1) d(20) f(3)
β	2.41%	1.60%	1.42%	0.96%
	s(22) p(0) d(78) f(0)	s(16) p(0) d(83) f(1)	s(15) p(0) d(83) f(1)	s(9) p(0) d(90) f(1)
σ (O \rightarrow Fe) ^b α	1.68%	1.94%	1.74%	1.82%
	s(94) p(3) d(2) f(1)	s(92) p(3) d(4) f(1)	s(92) p(3) d(4) f(1)	s(89) p(2) d(8) f(1)
β	13.43%	11.42%	10.13%	6.15%
	s(12) p(0) d(88) f(0)	s(19) p(0) d(81) f(0)	s(20) p(0) d(79) f(0)	s(23) p(1) d(76) f(0)

^aIn each row, the top number represents the contribution from all metal-centered orbitals, and the numbers below provides a breakdown into s, p, d, and f contributions from the metal in percent. ^bNot formally a bond. Metal character is related to the LMO orthogonality.

The qualitative assessment is supported by a more detailed analysis of the LMO compositions furnished by the NBO procedure (Table 3). The metal d character in the C–O π bond, oxygen nonbonding lone pair, and apparent Fe–O σ LMOs is notably larger in magnitude in the β set than in the α set. In particular, for the orbitals that afford Fe–O σ interactions, the contribution to the α -spin LMO is less than 2% metal (of which 90% has metal s character; the metal contribution likely represents nothing more than an orthogonalization tail of the ligand-centered LMO at the metal), whereas for the β -spin LMO it is over 10% metal (and primarily of Fe 3d character) for all calculations except HF. This represents the aforementioned partially covalent dative O \rightarrow Fe bonding character in the β orbital set. In the β -spin orbital set, the metal 3d character decreases noticeably with increasing HF exchange in the functional. In other words, how well the calculation performs with respect to experiment can be correlated with the metal d involvement in these LMOs which, in turn, correlates strongly with the trends for the HFCC analysis in Figure 3. Overall metal contributions decrease by about 1% from BP to B3LYP for the C–O π bond and oxygen lone pair, and by about 3% for the σ (O \rightarrow Fe) bond. This is significantly reduced further in the HF calculation. Results obtained with the long-range corrected LC-PBE0 are comparable to those from B3LYP calculations.

A qualitative molecular orbital diagram is shown in Figure 4. Consider a pseudo-octahedral complex where the five metal d

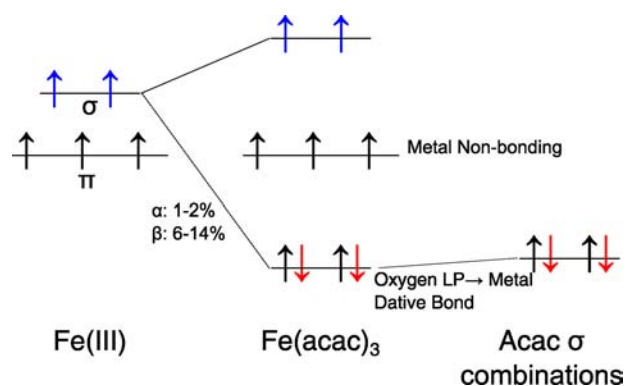


Figure 4. Qualitative orbital interaction diagram for Fe(acac)₃. The diagram is not drawn to scale, and energy differences between α and β orbitals are ignored to avoid clutter. Dative covalent oxygen–metal σ interactions may occur for β orbitals (red arrows). On the left-hand side, the metal ion is considered to be in the electrostatic field of the ligands, with nearly octahedral symmetry.

orbitals split in the electrostatic field of the ligands into those which are of local π symmetry with respect to the metal–oxygen bond (d_{xy} , d_{yz} , d_{xz}), and those that are of local σ

symmetry (d_z^2 , $d_{x^2-y^2}$). Metal orbitals of π symmetry (d_π) may interact with ligand π orbitals, as shown in the LMO plots provided in the SI. However, this interaction is expected to be weak and cause small effects on the HFCC,³⁴ which is confirmed by the LMO analysis of Table 2. As discussed above, a dative partially covalent O–Fe interaction may occur in the β set but is not permitted in the α set. The LMO analysis of the HFCC, the $E(N)$ plots, and the metal contributions to the ligand β -spin LMOs all point to the extent of covalency of these interactions and the resulting delocalization of β -spin density of the ligand to the metal as the source of the large methyl carbon HFCC and the strong overestimation of its pNMR shift by pure and low exact-exchange density functionals. Further, the mechanism causing the ligand pNMR shift in Fe(acac)₃ is best interpreted as resulting not so much from a delocalization of the metal-centered α -spin density onto the ligand, but rather via a delocalization of ligand-centered β -spin density to the metal which leaves excess α -spin density on the acac ligands (predominantly in the σ orbitals).

The question then arises as to what the correct amount of covalency in the metal–oxygen interactions should be. A related issue is that high exact exchange in the functional may deliver reasonable results regarding the covalency aspect, but as a result, it may lack sufficient electron correlation in order to produce reliable ligand HFCCs. Experimental data using infrared spectroscopy as well as magnetic techniques point to Fe–O bonds in Fe(acac)₃ that are almost entirely ionic.⁵⁷ That is, the appropriate amount of metal d character in the oxygen-centered LMOs should be small. Experimental evidence supports the correlation seen between metal d contributions in the occupied ligand β -spin LMOs and the degree by which the methyl carbon pNMR shift appears to be overestimated. Further details on the extent of the delocalization error are discussed in section 3.6 where calculations of the methyl carbon shifts with optimally tuned functionals are reported.

3.4. Chromium(III) Acetylacetonate. Cr(acac)₃ has been chosen as another target for a detailed analysis. Interestingly, for Cr(acac)₃, the methyl carbon pNMR shifts have opposite signs to those in Fe(acac)₃. Calculated and experimental chemical shifts are collected in Table 4. The calculated proton spectrum is in reasonable agreement with experiment and with theoretical data from the RB paper.³ As in the case of Fe(acac)₃, the shift for the problematic methyl carbon is too large in magnitude. However, the calculations are successful in the sense that the correct sign is obtained for this chemical shift. Compared to Fe(acac)₃, the absolute agreement with experiment is somewhat improved. Again, the closest calculated shifts are for B3LYP and HF, and the trend of increasing exact exchange in the functionals correlating with better agreement with experiment is evident. We note in passing that our calculated g-shifts are in reasonable agreement with experiment

Table 4. pNMR Shifts for Cr(acac)₃ Calculated with $S = 3/2$ and $T = 305$ K

	BP	PBE	B3LYP	PBE0	BHLYP	CAM	LC-PBE0	HF	RB ^a	expt
Δ_{iso}	−14.95	−15.11	−19.03	−19.98	−24.77	−20.07	−22.10	−33.66	−273.7	−11.65 ^b
methyl H	99.14	99.16	53.37	47.32	29.59	42.61	35.81	19.09	42.10	40.2 ^c
methyl C	−668.0	−705.5	−501.2	−540.4	−360.6	−440.3	−460.7	−328.9	−198.5	−130 ^c
methine H	63.83	63.96	42.17	40.80	25.58	31.85	27.78	17.11	35.68	30.2 ^d
methine C	254.9	236.2	279.7	225.5	249.0	250.4	188.0	158.0	269.5	
carbonyl C	1721	1776	1409	1375	1128	1267	1168	953.7	954.8	

^aGaussian 03/B3LYP, cc-pVTZ (C,H,O) 6-31G(d,p) (Cr). Reference 2. ^bReference 58. ^cIn CDCl₃, $T = 305$ K. Reference 15. ^dReference 2.

Table 5. Metal Contributions to Selected LMOs in Cr(acac)₃^a

	BP	LC-PBE0	BHLYP	HF
π (C–O) α	0.10% s(0) p(10) d(66) f(25)	0.17% s(0) p(4) d(82) f(14)	0.22% s(0) p(3) d(86) f(11)	0.42% s(0) p(2) d(92) f(6)
β	2.71% s(0) p(0) d(99) f(1)	2.13% s(0) p(0) d(99) f(1)	2.10% s(0) p(0) d(99) f(1)	1.75% s(0) p(0) d(98) f(1)
O LP α	0.57% s(47) p(2) d(49) f(2)	0.52% s(27) p(2) d(69) f(3)	0.54% s(22) p(2) d(74) f(3)	0.57% s(8) p(1) d(89) f(2)
β	2.65% s(12) p(0) d(87) f(1)	1.94% s(7) p(0) d(92) f(1)	1.74% s(7) p(0) d(92) f(1)	1.27% s(2) p(0) d(96) f(1)
σ (Cr–O) α	15.00% s(14) p(0) d(86) f(0)	12.44% s(17) p(0) d(83) f(0)	10.93% s(18) p(0) d(81) f(0)	7.39% s(18) p(0) d(82) f(0)
β	12.28% s(14) p(0) d(86) f(0)	10.22% s(19) p(0) d(81) f(0)	7.96% s(15) p(0) d(85) f(0)	6.88% s(20) p(0) d(80) f(0)

^aIn each row, the top number represents the contribution from all metal-centered orbitals, and the numbers below provides a breakdown into s, p, d, and f contributions.

(correct sign and order of magnitude). Similar to the iron complex, the *g*-shift for Cr(acac)₃ reported by RB indicates an overestimation of SO coupling.

LMO contributions to the methyl carbon HFCC are graphically displayed in Figure 6. Compositions of selected LMOs for Cr(acac)₃ are provided in Table 5. We discuss the LMO compositions first. The trends are comparable to those found for Fe(acac)₃ in the sense that little mixing of the occupied Cr d orbitals is seen in ligand-centered α orbitals, while slightly more mixing is found for the β C–O π bonding and the oxygen lone pair LMOs. Regarding the functional-dependence of the LMO compositions, the trend is similar to that of Fe(acac)₃ in that increasing exact exchange results in less metal d involvement in the C–O π and the oxygen nonbonding LP β -spin LMOs. There is a striking difference, however, in the metal d character in the Cr–O bonding orbitals. While the β set affords approximately the same amounts of metal d mixing for Cr(acac)₃ and Fe(acac)₃, involvement from the α set is much larger in Cr(acac)₃. The metal 3d contributions are in fact greater in magnitude here than those in the β set. There is a simple explanation for the difference between Cr and Fe: For Cr(III), both the α -spin and the β -spin d_{σ} are acceptor orbitals for dative bonds, while in high-spin Fe(III) only the β set is unoccupied. A qualitative orbital diagram for Cr(acac)₃ illustrating the situation is shown in Figure 5. The oxygen nonbonding lone pair is of π symmetry with respect to the metal center and therefore, like in Fe(acac)₃, can only interact with unoccupied d_{π}^{α} orbitals.

Unlike for Fe(acac)₃, the HFCC for the CH₃ carbon in the Cr complex is negative. Pure functionals overestimate the magnitude. This is ameliorated with the global hybrid and range-separated functionals. The analysis of the HFCC in terms of LMOs (Figure 6) shows that, along the functional series with increasing exact exchange, the contributions from the Cr–O σ bond as well as C–O and C–C nearest neighbor bonds do indeed become more positive (i.e., in the direction of better agreement with experiment). The oxygen lone pair contribution becomes more negative going from pure functionals to 100% HF exchange (as previously seen for Fe(acac)₃). The contributions from the nonbonding Cr 3d LMOs are negligible. It is emphasized that for most of the functionals the HFCC contributions from the O–Cr bonding LMOs are now negative. This sign change relative to Fe(acac)₃ reflects the larger Cr 3d _{σ} involvement in the α LMOs, which must be expected to leave an excess of β -spin density at least in parts of the ligands. For

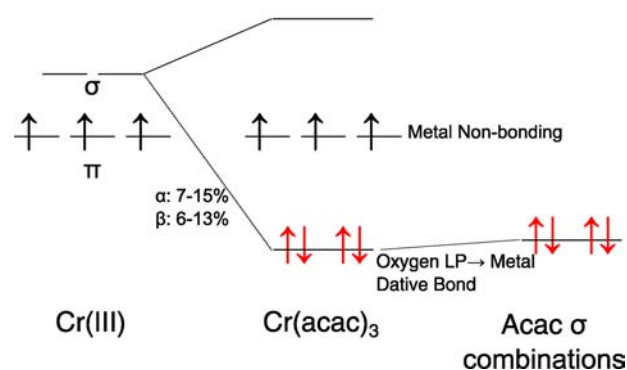


Figure 5. Qualitative orbital diagram for Cr(acac)₃. See also the caption of Figure 4. Dative covalent oxygen–metal σ interactions may occur for both α and β orbitals (red arrows).

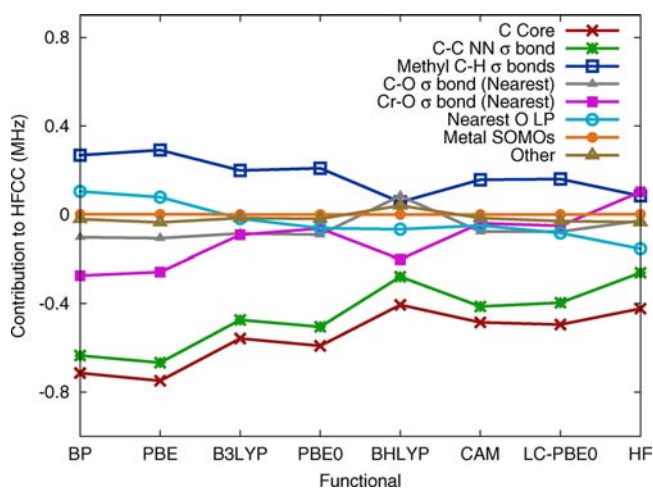


Figure 6. LMO contributions to the calculated methyl carbon HFCC for Cr(acac)₃.

BHLYP, the O–Cr bonding contributions decrease significantly compared to other functionals with similar amounts of exact exchange. However, this change is largely compensated by an accompanying increase in the negative HFCC contributions from the core orbitals and the C–C bond to the rest of the ligand, and from a sign change for the C–O σ bond. The source of this may be rooted in the LMO-generating procedure; see the Computational Details (section 2).

Table 6. pNMR Shifts for Ru(acac)₃ Calculated with $S = 1/2$ and $T = 305$ K

	BP	PBE	B3LYP	PBE0	BHLYP	CAM	LC-PBE0	HF	RB ^a	expt
Δg_{iso}	125.9	124.0	234.1	237.1	365.4	335.9	446.3	411.4	135.7	
methyl H	-15.26	-16.34	-17.97	-17.94	-14.11	-14.34	-13.18	-6.40	-15.30	-5.4, ^b -5.9 ^c
methyl C	-24.48	-28.58	-31.96	-41.23	-43.59	-41.73	-62.85	-66.05	-37.50	-21.3 ^b
methine H	-28.12	-27.80	-29.59	-29.31	-28.57	-30.70	-34.80	-25.73	-19.20	-29.4, ^b -29.9 ^c
methine C	410.3	440.5	428.3	413.0	401.3	364.6	311.8	375.3	438.2	139.4 ^b
carbonyl C	139.0	118.6	109.7	108.3	144.9	155.5	166.9	238.0	185.1	307.5 ^b

^aADF/ZORA SO (collinear)/BP86/TZ2P. Reference 3 ^bIn CDCl₃. $T = 305$ K. Reference 59. ^cAmbient temperature in D₂O. Reference 59.

When considering the results from the LMO analysis, the sign of the chemical shift, as well as the direction of the error in the calculated HFCC, may be assigned to the imbalance of metal d_{σ}^{α} and d_{σ}^{β} involvement in the dative O–metal σ bonds. As mentioned above, for Fe(acac)₃ only oxygen orbitals of β spin may interact with the Fe d_{σ} orbitals, leading to the positive methyl carbon pNMR shift and a positive sign of the deviations from experiment. For Cr(acac)₃, both α and β oxygen σ lone pairs may interact with Cr d_{σ} orbitals. From Table 5, covalent interactions between oxygen and the metal are stronger for the α set than for the β set. This imbalance causes excess β -spin density on the ligand and, as a result, a negative HFCC and a negative pNMR shift for the methyl carbon. The propensity for the ligand to donate stronger into the metal d_{σ}^{α} set has been rationalized previously by a qualitative argument based on the stability of high-spin versus low-spin d^5 configurations.¹⁴ The analysis supports the conclusion that DFT delocalization errors lead to an exaggerated covalency of ligand–metal bonding in both complexes, which creates too-large magnitudes of the HFCCs. The sign change of the pNMR methyl carbon shift between Fe(III) and Cr(III) is due to a lack of α -spin acceptor orbitals in the former case.

Since there is dative ligand–metal bonding in Cr(acac)₃ for both spins, there is a possibility of a partial compensation of errors. This is likely the reason why the absolute deviations between experiment and calculated methyl carbon shifts for Cr(acac)₃ are overall smaller than for Fe(acac)₃. On the basis of experimental data, the ligand–metal interaction in Cr(acac)₃ is more covalent than in Fe(acac)₃, and possibly affords some π backbonding.⁵⁷

3.5. Ru(acac)₃. The last system to be analyzed is Ru(acac)₃, the low-spin 4d analogue of Fe(acac)₃. The low-spin configuration reflects the stronger ligand-field splitting for the 4d complex. In D_3 symmetry, the occupied metal d orbitals belong to the a_1 or e irreducible representations. The Ru complex converged to spin-unrestricted solutions where the SOMO apparently derives from one of the e symmetry frontier orbitals. The Kohn–Sham single-determinant wave functions were symmetry-broken as a consequence, which required averaging of the calculated ligand chemical shifts for symmetry-equivalent atoms. The calculated shifts, experimental data, and calculated data from the literature (RB) are collected in Table 6. LMO contributions to the methyl carbon shifts are graphically displayed in Figure 7. As for the other metal complexes, the percentages of metal valence-d orbitals in the LMOs were determined; see Table 7 for the results for selected LMO sets.

As in Cr(III), the methyl carbon shifts in Ru(acac)₃ are negative. The calculations correctly reproduce this sign and the overall much smaller magnitude of this shift in the Ru complex, as well as the negative signs of the methyl and methine protons. The calculations further agree with experiment regarding the

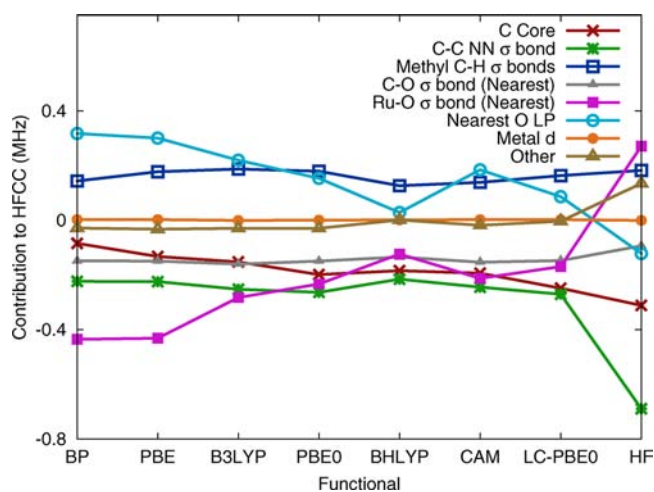


Figure 7. LMO contributions to the calculated methyl carbon HFCC for Ru(acac)₃.

positive signs of the remaining carbon shifts. The magnitudes of the calculated pNMR shifts overall match reasonably well with experiment except for the carbonyl carbons, where the shifts are severely underestimated by all calculations but HF. As far as the methyl carbon shifts are concerned, the density functionals now show an increased overestimation in magnitude relative to experiment as the fraction of exact exchange in the functional increases. In relative terms, the trend is pronounced. However, when considering the carbon chemical shift range among a larger set of acac complexes (in particular the calculated shift range), the variations are relatively minor. In this sense, most density functionals perform reasonably well for the Ru complex.

Turning to the extent of covalent interactions between the ligand and the metal, the data in Table 7 indicate a covalent character in the order Ru > Cr > Fe. The sign of the methyl carbon shift is caused by the larger d character of the α -spin σ (Ru–O) orbitals compared to their β -spin analogues, leaving excess β -spin density in the ligand σ -bonding framework; the rationale is similar to Cr(III) discussed above. Table 7 further shows that the imbalance between α - and β -spin for these orbitals is smaller than in the case of Cr, hence the overall smaller magnitude of the methyl carbon shift. The calculated pNMR shifts and the analysis are consistent with the fact that low-spin Ru(III) is only one electron away from a closed shell configuration. Moreover, unlike Cr(III) one should not expect the ligand to have a strong propensity for α - versus β -spin σ donation. The situation is qualitatively depicted in the form of an orbital diagram in Figure 8.

The LMO analysis of the methyl carbon HFCC, the results being graphically displayed in Figure 7, indicates that contributions from the oxygen lone pair, carbon core, and C–C σ bonding orbitals all trend more negative with increasing

Table 7. Metal Contributions to Selected LMOs in Ru(acac)₃^a

	BP	LC-PBE0	BHLYP	HF
π (C–O) α	0.07%	0.05%	0.05%	0.04%
	s(0) p(9) d(32) f(59)	s(0) p(10) d(18) f(71)	s(1) p(12) d(17) f(71)	s(1) p(11) d(19) f(69)
β	6.31%	1.62%	1.50%	0.98%
	s(0) p(0) d(96) f(3)	s(0) p(1) d(95) f(4)	s(0) p(1) d(95) f(4)	s(0) p(1) d(93) f(6)
O LP α	0.34%	0.24%	0.23%	0.17%
	s(79) p(1) d(14) f(6)	s(77) p(2) d(13) f(8)	s(76) p(2) d(13) f(8)	s(71) p(4) d(16) f(10)
β	0.86%	0.67%	0.61%	0.44%
	s(45) p(1) d(51) f(3)	s(41) p(1) d(54) f(4)	s(41) p(1) d(53) f(4)	s(37) p(2) d(56) f(5)
σ (Ru–O) α	15.41%	13.44%	12.58%	10.58%
	s(11) p(0) d(89) f(0)	s(13) p(0) d(86) f(0)	s(13) p(0) d(86) f(0)	s(16) p(0) d(84) f(0)
β	15.06%	12.83%	11.99%	9.80%
	s(11) p(0) d(89) f(0)	s(13) p(0) d(86) f(0)	s(13) p(0) d(86) f(0)	s(16) p(0) d(83) f(0)

^aIn each row, the top number represents the contribution from all metal-centered orbitals, and the numbers below provides a breakdown into s, p, d, and f contributions.

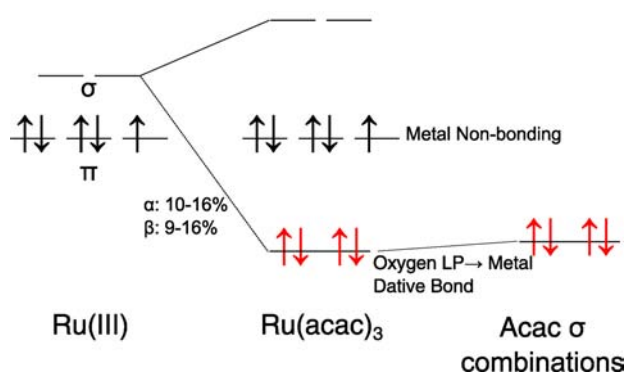


Figure 8. Qualitative orbital diagram for Ru(acac)₃. See also the caption of Figure 4. Dative covalent oxygen–metal σ interactions may occur for both α and β orbitals (red arrows).

fraction of exact exchange in the functional, which is partially offset by a significant positive trend from the O→Ru dative bonds. In contrast with Fe(acac)₃, but similar to Cr(acac)₃, there is no clear major trend in the LMO contributions with respect to the functional, with some contributions increasing and some decreasing as the percentage HF exchange is increased. This situation is partially a consequence of the delocalized electronic structure of the acac ligands. The important lesson learned from the LMO analysis is that the paired and unpaired Ru valence d spin orbitals contribute negligibly to the methyl carbon HFCCs, as they do in the Fe and Cr complexes. In other words, in all three cases the influence of the metal open shell on the distant ligand pNMR shifts is indirect, creating an α/β -spin imbalance in the ligand σ donation to the metal which ultimately determines the sign and magnitude of the contact shifts at the methyl carbons.

3.6. Optimal Tuning of the Functional for Fe(acac)₃. In this last subsection, we return to Fe(acac)₃ and ask the question whether the functional can be systematically improved and whether such a procedure results in a calculated methyl carbon pNMR shift closer to experiment. There has been significant activity in recent years aimed at optimally “tuning” hybrid functionals with range-separated exchange in an ab initio sense.^{48,54,60–63} Following our group’s recent work,⁵⁴ we use a 3-parameter expression⁶⁴ for the interelectronic distance in the exchange functional

$$\frac{1}{r_{12}} = \frac{\alpha + \beta \operatorname{erf}(\gamma r_{12})}{r_{12}} + \frac{1 - [\alpha + \beta \operatorname{erf}(\gamma r_{12})]}{r_{12}} \quad (2)$$

where the first term on the right-hand side is used for the long-range HF part. In eq 2, γ is the range-separation parameter. Further, α is the global HF fraction in the $\gamma \rightarrow 0$ limit, and $\alpha + \beta$ quantifies the fraction of HF exchange in the asymptotic limit at large interelectronic separations. The SI contains details about the procedure⁵⁴ which produces a set of different combinations of α , β , γ such that the functional satisfies the correct asymptotic behavior of the XC potential as well as the condition that the HOMO energy is the negative ionization potential, both for the neutral species and the anion. Among the parameter sets obtained in this way, one may further identify the functional with the least delocalization error, quantified by $E(\Delta N)$ (see section 3.2).

Table 8 list seven such parameter sets, together with calculated EPR parameters and the pNMR shieldings and

Table 8. Calculated Methyl Carbon ¹³C pNMR Data for Fe(acac)₃ Using Seven Functional Parametrizations That Satisfy the DFT Ionization Potential Condition (See SI) with Data Calculated with a Range-Separated Hybrid Variant of PBE. pNMR shifts for $S = 5/2$ and $T = 305$ K. $\Delta g_{\text{iso}} = g_{\text{iso}} - g_e$ in Parts per Thousand (ppt)

α	γ	Δg_{iso}	A_{iso}^a (MHz)	σ (ppm)	δ^d (ppm)
0.0659	0.200	7.24	1.83	−2054	2243
0.132	0.175	6.61	1.73	−1932	2121
0.193	0.150	5.97	1.64	−1813	2002
0.254	0.125	5.27	1.53	−1686	1876
0.307	0.100	4.64	1.44	−1575	1764
0.356	0.075	4.07	1.36	−1472	1662
0.399	0.050	3.57	1.28	−1386	1575
	expt	$\approx 0^b$			279.3 ^c

^aCorrected HFCC. See Computational Details (section 2). ^bReference 49. ^cIn CDCl₃. $T = 305$ K. Reference 15. ^dTMS ¹³C shielding constant calculated with LC-PBE0.

chemical shifts. Plots of $E(N)$ for the seven functionals, similar to the $E(N)$ plots of section 3.2, can be found in the SI. Similar to the global parametrizations of the various functionals used in section 3.2, increasing α leads to a decreasing methyl HFCC. At the same time, the curvature of $E(N)$ is the least for low values of α . The $E(N)$ curvatures for the optimally tuned LC-PBE0

variants are generally smaller than those of Figure 2. A caveat with the calculations is that for smaller α the ionization potential criterion is not as well satisfied as for large α , indicating that in the case of $\text{Fe}(\text{acac})_3$ it is difficult to satisfy the optimal tuning criteria simultaneously. It is therefore possible that the this long-range correction scheme in conjunction with the PBE exchange-correlation functional is simply not flexible enough to provide an accurate description of the electronic structure of $\text{Fe}(\text{acac})_3$, or that perhaps the correlation functional in PBE does not provide enough correlation in the optimally tuned versions. The case is reminiscent of the hierarchies in *ab initio* wave function methods: some molecules are reasonably well described at a lower-level correlation treatment, but other systems are not. Within the restrictions posed by the functional form adopted here (a hybrid GGA functional with range-separated exchange), the parameter sets of Table 8 are as optimal as possible as far as several energetic criteria rooted in DFT are concerned. Unless a description of the $\text{Fe}(\text{acac})_3$ electronic structure is out of reach with such a functional the results from this “tuning” section as well as the data of section 3.2 would indeed render the experimental estimate for the methyl pNMR shift somewhat suspicious (as previously suggested by Rastrelli and Bagno).

4. CONCLUSIONS

pNMR ligand chemical shifts have been calculated and analyzed for the three transition metal tris-acetylacetonato complexes $\text{Fe}(\text{acac})_3$, $\text{Cr}(\text{acac})_3$, and $\text{Ru}(\text{acac})_3$. The signs and magnitudes of the ligand chemical pNMR shifts are dominated by contact terms, and therefore they have the same signs as, and are proportional to, the magnitudes of, the isotropic HFCCs at the ligand nuclei. The signs and magnitudes of the ligand HFCCs are to a large extent driven by the extent of acac oxygen-to-metal σ donation involving unoccupied metal valence d_σ acceptor orbitals (the e_g set of d orbitals in octahedral parent symmetry). The role of delocalization of metal-centered spin density over the ligand atoms was found to play a very minor role.

Because of the spin-unrestricted nature of the calculations, the partially covalent character of the oxygen–metal bonding is best discussed in terms of pairs of α - and β -spin one-electron bonds rather than in terms of electron-pair bonding. A particular emphasis has been placed on the methyl carbon chemical shifts in the acac ligands. The results and the experimentally observed trends make intuitive sense: because high-spin iron(III) does not have formally unoccupied α -spin metal acceptor orbitals, dative ligand-to-metal bonding can only involve β -spin density, leaving an excess of α -spin density on the ligand. As a consequence, the methyl carbon pNMR shifts are large and positive. Cr(III) has both α - and β -spin acceptor d orbitals, as well as a propensity to accept ligand dative bonding more strongly in the α set. The result is an excess of β -spin density at the methyl carbon nuclei, and a negative methyl carbon pNMR chemical shift. Low-spin Ru(III) is similar to Cr(III) in this regard, but with a lesser preference for accepting α -spin over β -spin ligand donation. The methyl carbon pNMR shifts are negative, but smaller than for Cr(III).

Much of the analysis has focused on the role of the DFT delocalization error. In the acac complexes, π delocalization in the ligands is physically meaningful. The extent of covalency of the dative oxygen–metal bonds is seen to be driven by too much or too little delocalization, and therefore, it has a strong impact on the calculated ligand pNMR chemical shifts. For

Cr(III) and low-spin Ru(III) there is a degree of error cancellation present because metal acceptor orbitals of both spins are involved. A particularly problematic case is the methyl carbon shift of $\text{Fe}(\text{acac})_3$, for which most functionals produce shifts in excess of 1400 ppm (HF: about 800 ppm), whereas the experimental estimate is only around 279 ppm. As pointed out by Rastrelli and Bagno, the signal is probably too broad to obtain a reliable experimental shift. We have attempted to predict a “best” shift with optimally tuned range-separated hybrid functionals, which consistently place the methyl carbon shift well above 1500 ppm. If the delocalization error quantified by $E(\Delta N(\beta))$ for excess fractional electron numbers is a reliable criterion (it probes directly the problematic iron acceptor 3d orbitals), the most accurate electronic structure of $\text{Fe}(\text{acac})_3$ is obtained with functionals with low α (eq 2). These functionals give a lower limit of about 2000 for the methyl carbon shift. However, it is possible that the adopted functional form does not do justice to the complicated electronic structure of $\text{Fe}(\text{acac})_3$.

The data indicate other interesting trends in the acac complexes. For instance, for the carbon shifts in the acac backbone, which has a delocalized π system, the calculations produce shifts of the same sign as for the methyl carbon in the Fe complex (all positive), but of opposite sign in the Cr and Ru complex (methyl C negative, carbonyl and methine C positive). There is likely a spin-polarization mechanism present, i.e., the spin-density changes driven by the oxygen–metal σ interactions along with ligand–metal π interactions being a source of spin-density in the acac π system that may then in turn cause spin-polarization of the σ bonds in the ligand. A detailed analysis of this potentially complex mechanism is beyond the scope of this Article, but these trends certainly appear worthy of further study.

■ ASSOCIATED CONTENT

Supporting Information

Isosurface plots of selected LMOs for the tris-acetylacetonato complexes; TMS shielding values; a breakdown of methyl ^{13}C pNMR shifts into orbital, FC, and PC contributions; ZFS data; and additional information about the optimal tuning procedure of section 3.6. This material is available free of charge via the Internet at <http://pubs.acs.org>.

■ AUTHOR INFORMATION

Corresponding Author

*E-mail: jochena@buffalo.edu.

Notes

The authors declare no competing financial interest.

■ ACKNOWLEDGMENTS

This research was supported by the U.S. Department of Energy, Office of Basic Energy Sciences, Heavy Element Chemistry program under Grant DE-FG02-09ER16066. We acknowledge support by the Center for Computational Research (CCR) at the University at Buffalo. We thank Dr. Teemu Pennanen for providing a program to generate pNMR shift tensors with consideration of the ZFS tensor, which we used to verify our implementation. J.A. further thanks Prof. Martin Kaupp for constructive comments on a presentation of our findings at the 2012 CSC meeting in Calgary.

■ REFERENCES

- (1) Moon, S.; Patchkovskii, S. First-principles calculations of paramagnetic NMR shifts. In *Calculation of NMR and EPR Parameters. Theory and Applications*; Kaupp, M., Bühl, M., Malkin, V. G., Eds.; Wiley-VCH: Weinheim, 2004.
- (2) Rastrelli, F.; Bagno, A. *Chem.—Eur. J.* **2009**, *15*, 7990–8004.
- (3) Rastrelli, F.; Bagno, A. *Magn. Reson. Chem.* **2010**, *48*, S132–S141.
- (4) Bertini, I.; Luchinat, C.; Parigi, G. *Prog. Nucl. Mag. Reson. Spectrosc.* **2002**, *40*, 249–273.
- (5) Bertini, I.; Turano, P.; Vila, A. J. *Chem. Rev.* **1993**, *93*, 2833–2932.
- (6) Hrobarik, P.; Repisky, M.; Komorovsky, S.; Hrobarikova, V.; Kaupp, M. *Theor. Chem. Acc.* **2011**, *129*, 715–725.
- (7) Westler, W. M.; Lin, I.-J.; Perczel, A.; Weinhold, F.; Markley, J. L. *J. Am. Chem. Soc.* **2011**, *133*, 1310–1316.
- (8) Cohen, A. J.; Mori-Sánchez, P.; Yang, W. *Science* **2008**, *321*, 792–794.
- (9) Szilagy, R. K.; Metz, M.; Solomon, E. *J. Phys. Chem. A* **2002**, *106*, 2994–3007.
- (10) Ziegler, T. *J. Chem. Soc., Dalton Trans.* **2002**, 642–652.
- (11) Liimatainen, H.; Pennanen, T. O.; Vaara, J. *Can. J. Chem.* **2009**, *87*, 954–964.
- (12) Hrobárik, P.; Reviakine, R.; Arbuznikov, A. V.; Malkina, O. L.; Malkin, V. G.; Köhler, F. H.; Kaupp, M. *J. Chem. Phys.* **2007**, *126*, 024107–19.
- (13) Aquino, F.; Pritchard, B.; Autschbach, J. *J. Chem. Theory Comput.* **2012**, *8*, 598–609.
- (14) Eaton, D. R. *J. Am. Chem. Soc.* **1965**, *87*, 3097–3102.
- (15) Doddrell, D. M.; Gregson, A. K. *Chem. Phys. Lett.* **1974**, *29*, 512–515.
- (16) Autschbach, J.; Patchkovskii, S.; Pritchard, B. *J. Chem. Theory Comput.* **2011**, *7*, 2175–2188.
- (17) Kaupp, M.; Köhler, F. H. *Coord. Chem. Rev.* **2009**, *253*, 2376–2386.
- (18) Bühl, M. *Annu. Rep. NMR Spectrosc.* **2008**, *64*, 77–125.
- (19) Baerends, E. J., et al. *Amsterdam Density Functional; SCM, Theoretical Chemistry, Vrije Universiteit: Amsterdam, The Netherlands*; <http://www.scm.com>.
- (20) Becke, A. D. *Phys. Rev. A* **1988**, *38*, 3098–3100.
- (21) Perdew, J. P. *Phys. Rev. B* **1986**, *33*, 8822–8824.
- (22) van Lenthe, E.; Baerends, E. J.; Snijders, J. G. *J. Chem. Phys.* **1993**, *99*, 4597–4610.
- (23) Bylaska, E. J., et al. *NWChem, A Computational Chemistry Package for Parallel Computers, Version 6 (2012 Developer's Version)*; Pacific Northwest National Laboratory: Richland, Washington, 2011.
- (24) Valiev, M.; Bylaska, E. J.; Govind, N.; Kowalski, K.; Straatsma, T. P.; Dam, H. J. V.; Wang, D.; Nieplocha, J.; Apra, E.; Windus, T. L.; de Jong, W. A. *Comput. Phys. Commun.* **2010**, *181*, 1477–1489.
- (25) Nichols, P.; Govind, N.; Bylaska, E. J.; de Jong, W. A. *J. Chem. Theory Comput.* **2009**, *5*, 491–499.
- (26) Aquino, F.; Govind, N.; Autschbach, J. *J. Chem. Theory Comput.* **2010**, *6*, 2669–2686.
- (27) Aquino, F.; Govind, N.; Autschbach, J. *J. Chem. Theory Comput.* **2011**, *7*, 3278–3292.
- (28) Roos, B. O.; Lindh, R.; Malmqvist, P.; Veryazov, V.; Widmark, P. *J. Phys. Chem. A* **2005**, *109*, 6575–6579.
- (29) Kutzelnigg, W.; Fleischer, U.; Schindler, M. The IGLO-Method: Ab initio calculation and interpretation of NMR chemical shifts and magnetic susceptibilities. In *NMR Basic Principles and Progress*; Diehl, P., Fluck, E., Gunther, H., Kosfeld, R., Seelig, J., Eds.; Springer-Verlag: Heidelberg, Germany, 1990; Vol. 23; pp 165–262.
- (30) Autschbach, J.; Pritchard, B. *Theor. Chem. Acc.* **2011**, *129*, 453–466.
- (31) Moncho, S.; Autschbach, J. *J. Chem. Theory Comput.* **2010**, *6*, 223–234.
- (32) McConnell, H. M. *J. Chem. Phys.* **1956**, *24*, 764.
- (33) Eriksson, L. A. ESR hyperfine calculations. In *Encyclopedia of Computational Chemistry*; von Ragué Schleyer, P., Ed.; Wiley: Chichester, U.K., 1998; pp 952–958.
- (34) Rieger, P. H. *Electron Spin Resonance. Analysis and Interpretation*; The Royal Society of Chemistry: Cambridge, U.K., 2007.
- (35) Autschbach, J.; Ziegler, T. *Coord. Chem. Rev.* **2003**, *238/239*, 83–126.
- (36) Autschbach, J. Relativistic effects on magnetic resonance parameters and other properties of inorganic molecules and metal complexes. In *Relativistic Methods for Chemists*; Barysz, M., Ishikawa, Y., Eds.; Springer: Dordrecht, The Netherlands, 2010; Vol. 10; pp 521–598.
- (37) Glendening, E. D.; Badenhop, J. K.; Reed, A. E.; Carpenter, J. E.; Bohmann, J. A.; Morales, C. M.; Weinhold, F. *NBO 5.0*; Theoretical Chemistry Institute, University of Wisconsin: Madison, WI, 2001; <http://www.chem.wisc.edu/~nbo5>.
- (38) Weinhold, F. Natural bond orbital methods. In *Encyclopedia of Computational Chemistry*; von Ragué Schleyer, P., Ed.; John Wiley & Sons: Chichester, U.K., 1998; pp 1792–1811.
- (39) Autschbach, J.; Zheng, S.; Schurko, R. W. *Concepts Magn. Reson., Part A* **2010**, *36A*, 84–126.
- (40) Autschbach, J.; Zheng, S. *Magn. Reson. Chem.* **2008**, *46*, S48–S55.
- (41) Zheng, S.; Autschbach, J. *Chem.—Eur. J.* **2011**, *17*, 161–173.
- (42) Pennanen, T. O.; Vaara, J. *Phys. Rev. Lett.* **2008**, *100*, 133002–4.
- (43) Seth, M.; Ziegler, T. **2012**, *395*, 63–74.
- (44) Schmitt, S.; Jost, P.; van Wüllen, C. *J. Chem. Phys.* **2011**, *134*, 194113.
- (45) Becke, A. D. *J. Chem. Phys.* **1993**, *98*, 5648–5652.
- (46) Becke, A. D. *J. Chem. Phys.* **1993**, *98*, 1372–1377.
- (47) Yanai, T.; Tew, D. P.; Handy, N. C. *Chem. Phys. Lett.* **2004**, *393*, 51–57.
- (48) Srebro, M.; Autschbach, J. *J. Chem. Theory Comput.* **2012**, *8*, 245–256.
- (49) Hedewy, S.; Hoffmann, S. K. *Phys. Status Solidi A* **1986**, *97*, 129–133.
- (50) Johnson, A.; Everett, G. W. *J. Am. Chem. Soc.* **1972**, *94*, 1419–1425.
- (51) Reiher, M.; Salomon, O.; Hess, B. A. *Theor. Chem. Acc.* **2001**, *107*, 48–55.
- (52) Vlieg, R. M. E.; Zandstra, P. J. *Mol. Phys.* **1976**, *32*, 151–159.
- (53) Gregson, A. K.; Doddrell, D. M.; Bendall, M. R. *Aust. J. Chem.* **1979**, *32*, 1407–1414.
- (54) Srebro, M.; Autschbach, J. *J. Phys. Chem. Lett.* **2012**, *3*, 576–581.
- (55) Perdew, J. P.; Parr, R. G.; Levy, M.; Balduz, J. L., Jr. *Phys. Rev. Lett.* **1982**, *49*, 1691–1694.
- (56) Sharpe, P.; Richardson, D. E. *J. Am. Chem. Soc.* **1991**, *113*, 8339–8346.
- (57) Holm, R. H.; Cotton, F. A. *J. Am. Chem. Soc.* **1958**, *80*, 5658–5663.
- (58) Ikagawa, T.; Otsuka, T.; Kaizu, Y. *J. Phys. Chem. A* **1998**, *102*, 649–653.
- (59) Hoshino, Y.; Eto, M.; Fujino, T.; Yukawa, Y.; Ohta, T.; Endo, A.; Shimizu, K.; Sato, G. P. *Inorg. Chim. Acta* **2004**, *357*, 600–604.
- (60) Baer, R.; Livshits, E.; Salzner, U. *Annu. Rev. Phys. Chem.* **2010**, *61*, 85–109.
- (61) Stein, T.; Kronik, L.; Baer, R. *J. Chem. Phys.* **2009**, *131*, 244119(1)–244119(5).
- (62) Kuritz, N.; Stein, T.; Baer, R.; Kronik, L. *J. Chem. Theory Comput.* **2011**, *7*, 2408–2415.
- (63) Autschbach, J. *ChemPhysChem* **2009**, *10*, 1–5.
- (64) Yanai, T.; Tew, D. P.; Handy, N. C. *Chem. Phys. Lett.* **2004**, *393*, 51–57.